Cognitive Neurodynamics (2022) 16:391–399
https://doi.org/10.1007/s11571-021-09723-9

RESEARCH ARTICLE

Aberrant dynamic functional connectivity features within default mode network in patients with autism spectrum disorder: evidence from dynamical conditional correlation

Huibin Jia[1,2,3] · Xiangci Wu[1,2] · Enguo Wang[1,2]

Received: 7 April 2021 / Revised: 13 August 2021 / Accepted: 12 September 2021 / Published online: 4 October 2021

Abstract

Autism spectrum disorder (ASD) is characterized by aberrant functional connectivity (FC) within/between certain large-scale brain networks. Although relatively lower level of FC between default mode network (DMN) regions (i.e., DMN-FC) has been detected in many previous studies, they failed to capture the temporal dynamic features of DMN-FC and were limited by small sample size. Here, the dynamical conditional correlation, which could assess precise FC at each time point and has been proved to be a technique with high test–retest reliability, was applied to investigate the DMN-FC pattern of patients with ASD from the Autism Brain Imaging Data Exchange, which included functional and structural brain imaging data of more than 1000 participants. The data analysis here showed that compared to typical developing (TD) participants, patients with ASD exhibited significantly lower mean DMN-FC level across recording time, but significantly higher variance of DMN-FC level across recording time. Moreover, these alterations were significantly associated with symptom severity of patients, especially their impaired communication skills and repetitive behaviors. These results support the view that aberrant temporal dynamic of FC within DMN is an important neuropathological feature of ASD and is a potential biomarker for ASD diagnosis.

Keywords Dynamic functional connectivity · Dynamical conditional correlation · Autism spectrum disorder · Default mode network

Introduction

Autism spectrum disorder (ASD), refers to a broad range of conditions characterized by challenges with social and verbal/nonverbal communication skills and repetitive behaviors (Anagnostou and Taylor 2011). According to the 2016 data of Autism and Developmental Disabilities Monitoring Network which is an active surveillance program that provides estimates of the prevalence of ASD in United States, the ASD prevalence was 18.5 per 1000 (one in 54) children aged 8 years, and ASD was 4.3 times as prevalent among boys as among girls (Baio et al. 2018). This neuropsychiatric disorder is generally diagnosed in early childhood and brings heavy burden to the affected individuals and their caregivers (Leigh and Du 2015).

Due to the application of the newly developed neuroimaging techniques, scientists have got a deep insight into the neural mechanisms that underpin this disorder (Amaral et al. 2008; Walsh et al. 2021). Using functional magnetic resonance imaging (fMRI), researchers revealed that ASD was accompanied by aberrant functional connectivity (FC) between distinct cortical regions (Sun et al. 2021). This abnormal FC could be cortical hyperconnectivity or hypoconnectivity, depending on various factors (e.g., the large-scale brain network being investigated and task being executed) (Jung et al. 2014; Kana et al. 2015;

Huibin Jia and Xiangci Wu have contributed equally to this work.

✉ Huibin Jia
huibin_jia@foxmail.com

✉ Enguo Wang
enguowang@126.com

[1] Institute of Psychology and Behavior, Henan University, Kaifeng 475004, China

[2] School of Psychology, Henan University, Kaifeng 475004, China

[3] Institute of Cognition, Brain and Health, Henan University, Kaifeng 475004, China

Keehn et al. 2013). In the current study, we focus on the FC within default mode network (DMN) which plays crucial role in mentalizing, self-reference and social cognition, since hypoconnectivity between DMN regions is among the most commonly reported findings in patients with ASD (Padmanabhan et al. 2017). Although hypoconnectivity within DMN has been consistently observed in previous studies, the defects of these studies may seriously hinder the discovery of precise FC pattern within DMN. Firstly, static Pearson correlation coefficient between fMRI signals of different brain regions was commonly used as measure in previous ASD-related FC studies (Keehn et al. 2013; Lawrence et al. 2019). However, it has been shown that the coupling or dependency between cortical regions fluctuated over time, even during task-free resting-state, thus static FC may be too simplistic to capture the full extent of cortical activities (Li et al. 2020). The sliding-window based techniques, in which correlation matrices are computed over fixed-length windowed segments of the neural time series, have been applied to track the dynamic nature of FC in some previous studies (Falahpour et al. 2016). Note that, these techniques have certain limitations, e.g., the window length was arbitrarily decided by researchers, unable to reflect transient FC mode, and low or moderate test–retest reliability (Choe et al. 2017). Secondly, the sample size was very small in previous studies (i.e., < 100) (Falahpour et al. 2016; Jung et al. 2014). Considering these shortcomings, the dynamical conditional correlation (DCC), which could assess the dynamic functional connectivity (dFC) between brain areas and has been proved to be a FC technique with relatively higher test–retest reliability than traditional sliding-window approach (Choe et al. 2017), was applied to investigate the DMN-FC (i.e., the functional connectivity between DMN regions) patterns of patients with ASD. The datasets from the Autism Brain Imaging Data Exchange (ABIDE), which included functional and structural brain imaging data of more than 1000 participants, were used here (Di Martino et al. 2014). We hypothesized that compared to typical developing (TD) participants, patients with ASD should exhibit significantly lower average DMN-FC level across recording time which is consistent with previous studies, but significantly higher variation of DMN-FC level across recording time. Moreover, these abnormalities should be significantly associated with the autistic symptom severity in ASD group.

Materials and methods

The selection of fMRI datasets

ABIDE consists of 1112 resting-state functional magnetic resonance imaging datasets with corresponding structural MRI and phenotypic information (e.g., gender, age at scan, sex, IQ and diagnostic information) of 539 patients with ASD and 573 TD participants (Di Martino et al. 2014). These datasets were collected from 17 international sites, and have been anonymized in accordance with the Health Insurance Portability and Accountability Act guidelines and 1000 Functional Connectomes Project/International Neuroimaging Data-sharing Initiative protocols. The data collection was carried out in accordance with the basic principles of the Helsinki declaration and approved by the research ethics committees of 17 institutions (i.e., California Institute of Technology/Carnegie Mellon University/Kennedy Krieger Institute/Ludwig Maximilians University Munich/NYU Langone Medical Center/Olin Center, Institute of Living at Hartford Hospital/Oregon Health and Science University/San Diego State University/BCN NeuroImaging Center, University Medical Center Groningen/Stanford University/Trinity Centre for Health Sciences/University of California, Los Angeles/University of Leuven/University of Michigan/University of Pittsburgh/University of Utah/Yale Child Study Center). Informed consent was obtained from the participants or their legal guardians. Details of acquisition and site-specific protocols are available at .

Imaging analyses here were limited to: (1) data with anatomical images providing near-full brain coverage and successful registration; (2) data passing manual quality assessments of three independent raters; (3) data with Mean Framewise Displacement (func_mean_fd) < 0.2 mm; (4) individuals with Percent Framewise Displacement (FD) greater than 0.2 mm (func_perc_fd) $< 25\%$; (5) individuals with IQ > 75; (6) individuals in ASD group with reliable diagnostic information obtained via Autism Diagnostic Observation Scale (ADOS) or Autism Diagnostic Interview-Revised (ADI-R); (7) data from sites with more than three participants in each group after selecting datasets based on the above six criteria. Finally, the datasets of 343 patients with ASD and 428 TD participants were retained. Statistical tests conducted on the age at scan, func_mean_fd, func_perc_fd and IQ score did not reveal any significant group difference ($ps > 0.05$).

Signal preprocessing

The fMRI signal preprocessing was performed using the Data Processing Assistant for Resting-State fMRI (DPARSF) (Yan and Zang 2010), which is a convenient plug-in software based on Statistical Parametric Mapping (SPM) package and Resting-State fMRI Data Analysis Toolkit (REST) (Friston et al. 1995; Song et al. 2011). The following sequence of preprocessing steps was performed:

1. The first 4 image volumes were discarded to allow the fMRI signal to reach a steady state.
2. Slice-timing correction. All volume slices were corrected for different signal acquisition times by shifting the signal measured in each slice relative to the acquisition of the slice at the mid-point of each TR.
3. The images for each subject were realigned using a six-parameter (rigid body) linear transformation with a two-pass procedure (registered to the first image and then registered to the mean of the images after the first realignment).
4. Individual structural images (T1-weighted MPRAGE) were co-registered to the mean functional image after realignment using a 6 degrees-of-freedom linear transformation without re-sampling.
5. The transformed structural images were segmented into grey matter, white matter and cerebrospinal fluid (Ashburner and Friston 2005). The Diffeomorphic Anatomical Registration Through Exponentiated Lie algebra (DARTEL) tool was used to compute transformations from individual native space to MNI space (Ashburner 2007).
6. The Friston 24-parameter model was used to regress out head motion effects from the realigned data (Friston et al. 2008).
7. The signals from WM and CSF were regressed out to reduce respiratory and cardiac effects. Global signal regression did not conducted, since previous studies showed that it could yield substantial increases in negative correlations (Murphy et al. 2009).
8. The images were registered into Montreal Neurological Institute (MNI) space with 3 mm^3 cubic voxels by using transformation information acquired from DARTEL. The images were further smoothed by a kernel of 6 mm.
9. Temporal filtering (0.01–0.1 Hz) was performed on the time series in order to remove low-frequency drifts and high-frequency noise from the signal.
10. According to Andrews-Hanna et al. (2010), 18 sphere regions-of-interest (ROIs) with radius 10 mm within DMN were defined. The centroid coordinate of each sphere ROI was displayed in Table 1 (Andrews-Hanna et al. 2010). The signal time series of each ROI was computed as the mean value of voxels within this ROI.

Computing dFCs

Here, the dFC metrics between ROIs were computed through the DCC method. Compared to the traditional and widely used sliding-window method, the DCC method is a model-based multivariate volatility method that has consistently been shown to outperform sliding-window methods (Choe et al. 2017). The DCC method at least has the following advantages. Firstly, it does not need to choose a window length, which is usually arbitrarily decided by researchers. Secondly, it provides a more suitable estimate of the correlation at a specific time point, which can be critical particularly if it is important to link the dynamic correlation to the timing of a specific task or emotion and can reflect abrupt changes in connectivity patterns. Thirdly, the test–retest reliability of DCC method is much higher than the sliding-window methods (Choe et al. 2017).

Assume y_t is bivariate mean zero time series of two ROIs with dimension 2 × T, where T is the length of each ROI signal. The dynamic correlations R_t with dimension 1 × T can be calculated using the following equations:

$$\sigma_{i,t}^2 = \omega_i + \alpha_i \cdot y_{i,t-1}^2 + \beta_i \cdot \sigma_{i,t-1}^2, \quad \text{where i equals 1 or 2} \tag{1}$$

$$D_t = diag\{\sigma_{1,t}, \sigma_{2,t}\} \tag{2}$$

$$\varepsilon_t = D_t^{-1} \cdot y_t \tag{3}$$

$$Q_t = (1 - \theta_1 - \theta_2) \cdot \overline{Q} + \theta_1 \cdot \varepsilon_{t-1} \cdot \varepsilon_{t-1}^{'} + \theta_2 \cdot Q_{t-1} \tag{4}$$

$$R_t = diag\{Q_t\}^{-1/2} \cdot Q_t \cdot diag\{Q_t\}^{-1/2} \tag{5}$$

Firstly, each ROI signal within y_t is modeled by a generalized autoregressive conditional heteroscedastic (GARCH) model, which expresses the conditional variance of a single time series at time t as a linear combination of past values of the conditional variance and of the squared process itself (Eq. (1)). Secondly, the standardized residual ε_t was computed through Eqs. (2) and (3). Thirdly, non-normalized version of the time-varying correlation matrix Q_t was computed using an exponentially weighted moving average (EWMA) window (Eq. (4)). Note that, in Eq. (4), θ_1 and θ_2 are non-negative scalars satisfying $0 < \theta_1 + \theta_2 < 1$, $\overline{Q}$ can be calculated as $\overline{Q} = \frac{1}{T}\sum_{t=1}^{T} \varepsilon_t \cdot \varepsilon_t^T$. Lastly, Q_t is rescaled, which creates the dynamic correlations R_t.

Computing temporal mean and variance of dFCs

After the dFCs of all ROI pairs were assessed through the approach illustrated above, we could obtain a time-varying correlation matrix C_t with dimension N × N × T, where N and T were the number of ROIs and time points respectively. Thus this C_t could reflect the FC between each ROI pair at each time point. In this study, we computed two basic summary statistics for each pairwise dFC, i.e., the temporal mean value of dFC ($\overline{FC}$) and the temporal variance over time (FC_δ).

Table 1 The 18 ROIs within DMN defined in the current study

ROI	Abbrev	Brodmann area	MNI coordinate		
			x	y	z
PCC-aMPFC core					
Anterior medial prefrontal cortex (#1)	aMPFC	10, 32	− 6	52	− 2
Posterior cingulate cortex (#2)	PCC	23, 31	− 8	− 56	26
dMPFC subsystem					
Dorsal medial prefrontal cortex (#3)	dMPFC	9, 32	0	52	26
Left temporal parietal junction (#4)	lTPJ	40, 39	− 54	− 54	28
Left lateral temporal cortex (#5)	lLTC	21, 22	− 60	− 24	− 18
Left temporal pole (#6)	lTempP	21	− 50	14	− 40
Right temporal parietal junction (#7)	rTPJ	40, 39	54	− 54	28
Right lateral temporal cortex (#8)	rLTC	21, 22	60	− 24	− 18
Right temporal pole (#9)	rTempP	21	50	14	− 40
MTL subsystem					
Ventral medial prefrontal cortex (#10)	vMPFC	11, 24, 25, 32	0	26	− 18
Left posterior inferior parietal lobule (#11)	lpIPL	39	− 44	− 74	32
Left retrosplenial cortex (#12)	lRsp	29, 30, 19	− 14	− 52	8
Left parahippocampal cortex (#13)	lPHC	20, 36, 19	− 28	− 40	− 12
Left hippocampal formation (#14)	lHF^{+}	20, 36	− 22	− 20	− 26
Right posterior inferior parietal lobule (#15)	rpIPL	39	44	− 74	32
Right retrosplenial cortex (#16)	rRsp	29, 30, 19	14	− 52	8
Right parahippocampal cortex (#17)	rPHC	20, 36, 19	28	− 40	− 12
Right hippocampal formation (#18)	rHF^{+}	20, 36	22	− 20	− 26

Statistical tests on temporal mean and variance of dFCs

In order to test whether the two summary statistics of dFC (i.e., $\overline{FC}$ and FC_{δ}) were significantly altered in patients with ASD, the network-based statistic (NBS) was conducted (Zalesky et al. 2010). This method consists of following steps. Firstly, mass univariate testing was performed on all the 153 (i.e., C_{18}^{2}) pairs on a graph via independent-samples t-test, with the age at scan, func_mean_fd, func_perc_fd, IQ score, gender and sites included as covariates. Secondly, the pairs with t-test value exceeding a given threshold ($p < 0.005$) were admitted to a set of supra-threshold pairs. Thirdly, "connected graph components" defined as a set of supra-threshold pairs for which a path can be found between any two ROIs within this component were identified. The size of each component was assessed as the total number of pairs it comprised. Fourthly, the null distribution of size of connected component was empirically derived using a permutation approach with 5000 permutations. For each permutation, all participants were randomly re-allocated into two groups, and the above three steps were conducted. The component with largest size was recorded for each permutation, which yielded an empirical null distribution for the size of the largest component. Lastly, the one-sided family-wise error rate corrected p-value for an originally identified component was estimated as the proportion of permutations for which the largest component was of the same size or greater.

Correlations with symptom severity

In order to investigate the relationship between the two summary statistics and measures of autistic symptom severity in the ASD group, the Pearson correlation coefficients between the two summary statistics and symptom severity as assessed by the ADOS total (ADOS_TOTAL), communication (ADOS_COMM), social (ADOS_SOCIAL) and stereotyped behavior (ADOS_STEREO_BEHAV) scores were calculated for each ROI pair after controlling the effects of following variables: the age at scan, func_mean_fd, func_perc_fd, IQ score, gender and sites. The significance of the correlation coefficients was assessed with t-statistic. The threshold for significance was $p < 0.05$.

Classification of participants in ASD group and TD group using support vector machine

Note that the above statistical tests and correlation analyses could be applied to reveal the neuropathlogical mechanism

of autism, and were inadequate to assist in clinical diagnostic purposes. For clinical diagnostic decision, biomarkers with the ability to reliably distinguish normal from abnormal at the individual participant level should be developed and validated. To achieve this purpose, we developed a classification method with support vector machine (SVM) to distinguish ASD patients with healthy controls at individual participant level.

The features used in the SVM were temporal mean and variance of dFCs with significant group differences as revealed by NBS.

The SVM performs classification by finding the hyperplane that maximizes the margin between the two classes. Here, a Radial Basis Function (RBF) kernel was used. In order to assess the generalization performance of the SVM model, a fivefold cross-validation strategy was adopted. In the strategy, all the participants in two groups were partitioned into 5 subsets (each subset with a roughly equal sample size). Moreover, the participant numbers of two groups were roughly equal in each subset. In each run, the samples within one subset were used as the testing dataset, while the remaining samples in the other 5 subsets are used as the training dataset. The averaged value of classification results across all fivefold cross-validations were reported here.

Before training an SVM with the RBF kernel, two hyper-parameters should be defined: C and gamma. A nested cross-validation strategy was used to identify the optimal values of these two hyper-parameters within range [2^{-5}, 2^{-4}, 2^{-3}, …, 2^{4}, 2^{5}]. Firstly, the training dataset in each run was further split into training subset and testing subset. Secondly, for each combination of values for hyper-parameters, SVM was trained on the training subset and validated on the testing subset. This procedure was repeated for 5 times. The average classification accuracy under a specific combination of hyper-parameter values was then computed. For each run, the hyper-parameter values combination with the highest average classification accuracy were chosen and applied to construct the SVM model using the training dataset.

Results

Group differences on the temporal mean of dFCs

Statistical tests conducted on the temporal mean of dFC (i.e., $\overline{FC}$) revealed that the $\overline{FC}$ of certain connections were significantly lower in ASD group, compared to those in TD group. These results included: (1) the $\overline{FC}$ of dFCs between ROI #1 (anterior medial prefrontal cortex, aMPFC) and ROI #2 (posterior cingulate cortex, PCC), ROI #3 (dorsal medial prefrontal cortex, dMPFC), ROI #7 (temporal parietal junction [right hemisphere], rTPJ), ROI #9 (temporal pole [right hemisphere], rTempP), ROI #10 (ventral medial prefrontal cortex, vMPFC), ROI #12 (retrosplenial cortex [left hemisphere], lRsp); (2) the $\overline{FC}$ of dFCs between ROI #2 (PCC) and ROI #3 (dMPFC), ROI #9 (rTempP); (3) the $\overline{FC}$ of dFC between ROI #3 (dMPFC) and ROI #4 (temporal parietal junction [left hemisphere], lTPJ); (4) the $\overline{FC}$ of dFC between ROI #7 (rTPJ) and ROI #13 (parahippocampal cortex [left hemisphere], lPHC). From these results, we could find that significantly reduced $\overline{FC}$ mainly involved ROI #1 (aMPFC), ROI #2 (PCC) and ROI #3 (dMPFC). The numbers of aberrant connections for these 3 ROIs were 6, 3 and 3 respectively.

Group differences on the temporal variance of dFCs

Statistical tests conducted on the temporal variance of dFC (i.e., FC_{δ}) revealed that the FC_{δ} of two connections were significantly higher in ASD group, compared to those in TD group. These two connections were the dFC between ROI #1 (aMPFC) and ROI #2 (PCC), and the dFC between ROI #1 (aMPFC) and ROI #12 (lRsp).

Associations between the temporal mean of dFCs and autistic symptom severity

Through computing the correlation between $\overline{FC}$ of each connection and autistic symptom severity assessed by ADOS, we found that: the Pearson correlation coefficients between $\overline{FC}$ of certain connections and ADOS_COMM score, ADOS_STEREO_BEHAV score were significantly negative. Significant results were not found for the other two scores (i.e., ADOS_TOTAL and ADOS_SOCIAL).

The correlations of ADOS_COMM score and $\overline{FC}$ of the following connections were significantly negative: the dFC between ROI #2 (PCC) and ROI #4 (lTPJ), the dFC between ROI #12 (lRsp) and ROI #14 (hippocampal formation [left hemisphere], lHF^{+}). Please refer to Table S1 of supplementary materials for details.

As for ADOS_STEREO_BEHAV score, negative correlations were found for quite a few connections. Please refer to Table S2 of supplementary materials for details. After summarizing the results, we could find that the ROIs with significant connections larger than 3 were ROI #12 (lRsp), ROI #14 (lHF^{+}) and ROI #9 (rTempP).

These results were displayed in Fig. 1.

Associations between the temporal variance of dFCs and autistic symptom severity

Analyzing the relationship between FC_δ of ROI pairs and ADOS scores, significantly positive correlations were found for ADOS_COMM, ADOS_STEREO_BEHAV, but not for ADOS_TOTAL and ADOS_SOCIAL.

Significantly positive correlations were detected for plenty of connections when testing the relationship between FC_δ of ROI pairs and ADOS_COMM score. Please refer to Table S3 of supplementary materials for details. Observing the results, we found that these connections were mainly contributed by the following ROIs: ROI #4 (lTPJ), ROI #12 (lRsp) and ROI #14 (lHF$^+$). The number of significant ROI pairs for these three ROIs were 14, 12 and 8.

As for ADOS_STEREO_BEHAV, we found that the correlation between ADOS_STEREO_BEHAV score and FC_δ of ROI pairs ROI #1 (aMPFC)-ROI #3(dMPFC) was significant ($p < 0.05$). Please refer to Table S4 of supplementary materials for details.

These results were displayed in Fig. 2.

The classification result of SVM

The features used in the SVM were temporal mean and variance of dFCs with significant group differences as shown in "Group differences on the temporal mean of dFCs" and "Group differences on the temporal variance of dFCs" sections. The final results showed that the classification accuracy rate has its maximum 83.27% (implying that the classification error rate is 16.73%). This implies that we have obtained a meaningful diagnostic result using the suggested techniques.

Discussion

In the current study, using DCC technique and the resting-state fMRI datatsets of ABIDE, the hypothesis that temporal mean and variance of dFCs within DMN were altered in patients with ASD was validated. Moreover, through classification analysis, we found that these significantly altered FC metrics could be used in ASD diagnosis with high classification accuracy (83.27%). In the other hand, through correlation analysis, we found that these alterations could predict the autism symptom severity of patients.

Altered dFCs features within DMN

Statistical tests conducted on $\overline{FC}$ of dFCs revealed that the $\overline{FC}$ of many ROI pairs in ASD group were significantly smaller than that in TD group. Observing the aberrant connections, we found that they mainly involved the following ROIs: anterior medial prefrontal cortex (aMPFC), posterior cingulate cortex (PCC) and dorsal medial prefrontal cortex (dMPFC). The aMPFC, especially its dorsal section, is supposed to be involved in self-referential processes (Shalom 2009). The PCC, together with its adjacent retrosplenial cortex (Rsp), is consistently engaged by a range of tasks that examine episodic memory, including autobiographical memory and imagining the future, spatial navigation and also scene processing (Auger and Maguire 2013; Leech and Smallwood 2019). The dMPFC may contribute to the development of the tendency to initiate joint attention in infancy, thus its dysfunction is followed by impairments in the development of social cognition, as assessed on theory of mind measures (Vargas et al. 2019). Theories suggest that the MPFC and PCC together form a

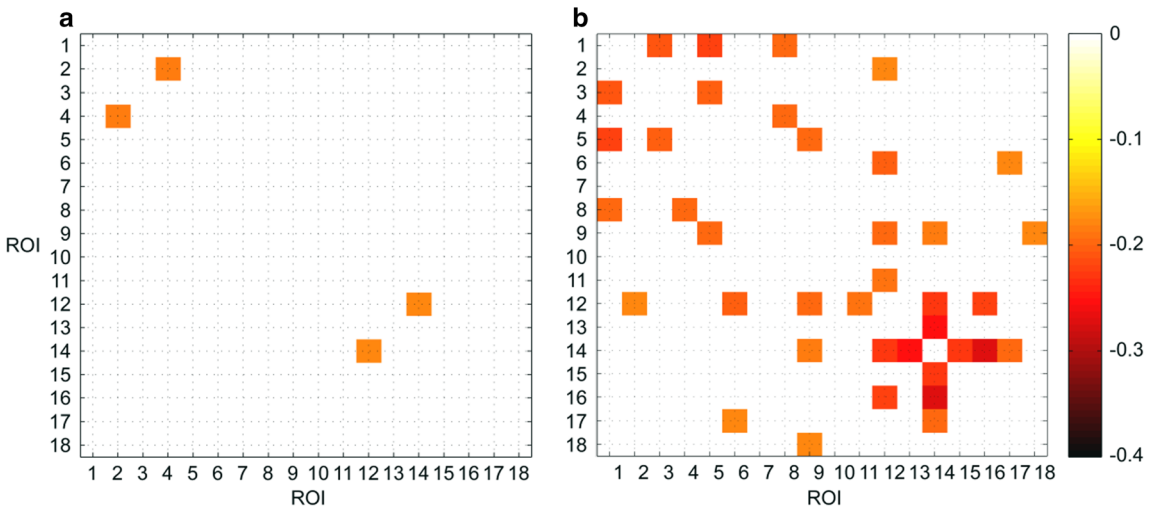

Fig. 1 The correlation coefficient between temporal mean of dFCs and autistic symptom severity assessed by ADOS_COMM (**A**) and ADOS_STEREO_BEHAV (**B**). Note that only connections with significant correlation coefficients were shown

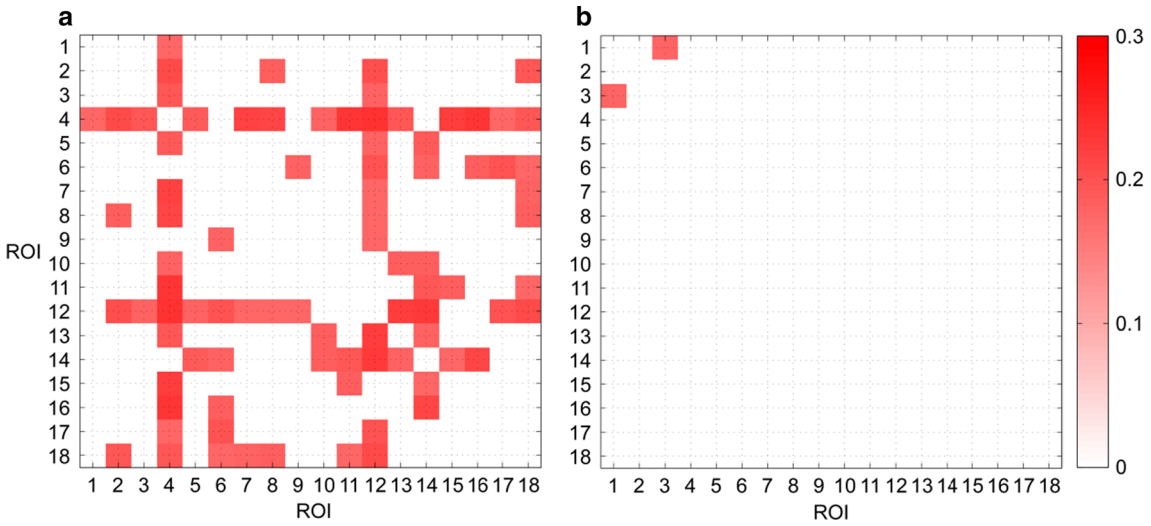

Fig. 2 The correlation coefficient between temporal variance of dFCs and autistic symptom severity assessed by ADOS_COMM (**A**) and ADOS_STEREO_BEHAV (**B**). Note that only connections with significant correlation coefficients were shown

core network dedicated to reflecting upon ourselves, encoding and retrieving information about ourselves.

Further statistical tests over FC_δ also revealed the crucial role of aMPFC and PCC/Rsp on brain connectivity: FC_δ of dynamic aMPFC-PCC connectivity and aMPFC-lRsp connectivity were significantly larger in ASD group, compared with those in TD group.

Here, hypoconnectivity were found for the links between aMPFC/dMPFC, PCC and other DMN areas which were highly consistent with previous studies using traditional statics FC techniques (Padmanabhan et al. 2017). However, a novel finding here is that the temporal variance of dFCs between aMPFC and other DMN regions (i.e., PCC/lRsp) were significantly higher in ASD group, which has not been detected via traditional approaches. These results suggested that significantly much lower and more volatile connections between DMN regions, especially those involved aMPFC/dMPFC and PCC/Rsp, were an important pathological feature of ASD, which may reduce the efficiency of functions related with DMN, such as self-representation, social information processing.

Correlations between dFCs features and symptom severity

The speculation made above was further supported by the correlation analysis between dFC summary statistics and measures of autistic symptom severity in the ASD group: negative correlations between $\overline{FC}$ and ADOS scores, positive correlations between FC_δ and ADOS scores.

The correlations between ADOS_COMM score and $\overline{FC}$ of the following two ROI pairs were significantly negative: the dFC between ROI #2 (PCC) and ROI #4 (lTPJ), the dFC between ROI #12 (lRsp) and ROI #14 (lHF^+). Summarizing the connections whose FC_δ were positively associated with ADOS_COMM score, we found that these significant results were mainly contributed by the following ROIs: ROI #4 (lTPJ), ROI #12 (lRsp) and ROI #14 (lHF^+). These results suggested that the abnormal level of features of connections involved lTPJ, lRsp and lHF^+, whether their temporal mean or variances, could result in the impairment of communication skills in patients with ASD. A very striking finding observed here was that the correlation of ADOS_COMM score and FC_δ of 14 dFCs involved lTPJ were significantly positive, which means that the correlations of ADOS_COMM score and FC_δ of only three lTPJ-related dFCs did not reach significant level. These results highlighted the importance of lTPJ in social communication development. Previous studies suggested that the TPJ is associated with joint attention, generating shared focus on an object across individuals for understanding, and predicting others' actions and intentions (Goelman et al. 2019). Our results observed here is highly consistent with these previous theories.

Here, the correlations between ADOS_STEREO_BEHAV score and $\overline{FC}$ of many ROI pairs were significantly negative, and we could find that these ROIs with significant connections larger than 3 were ROI #12 (lRsp), ROI #14 (lHF^+) and ROI #9 (rTempP). On the other hand, significant correlation between ADOS_STEREO_BEHAV score and FC_δ was only found for the connection between ROI #1 (aMPFC) and ROI #3 (dMPFC), i.e., the connection within MPFC. Similar to the results on ADOS_COMM score, the results on ADOS_STEREO_BEHAV score also highlighted the importance of ROI #12 (lRsp) and ROI #14 (lHF^+). The retrosplenial cortex has emerged as a key

member of a core network of brain regions that underpins a range of cognitive functions, including episodic (autobiographical) memory, spatial navigation, imagination and planning for the future (Vann et al. 2009). The hippocampal formation is part of medial temporal lobes and is essential for spatial navigation, as well as the formation of new declarative and episodic memories (Lee et al. 2019; Sabariego et al. 2020).

Observing the patterns of results of correlation analysis, we could find a very interesting phenomenon: when analyzing the $\overline{FC}$ of dFCs, more significant ROI pairs were found for ADOS_STEREO_BEHAV score, compared with ADOS_COMM score; whereas when the FC_{δ} of dFCs were investigated, opposite pattern appeared. This amazing result may suggest that in patients with ASD, relatively lower information exchange efficiency between cortical regions may result in repetitive behaviors, whereas relatively higher variability of information exchange efficiency between cortical regions may impair the verbal/nonverbal communication skills of human beings.

Future directions in related field

The static or dynamic FCs between time series of ROI pairs through classical Pearson's correlation or DCC techniques were considered to be low-order representation of the functional interaction. In order to comprehensively characterize the functional networks under normal or abnormal states, multi-level, high-order FC networks have been proposed by previous researchers (Zhang et al. 2017). Zhang et al. (2016) proposed that higher FC network could be computed based on the principle of "correlation's correlation" (Zhang et al. 2016). In this approach, the traditional FCs between any cortical ROI pair produced FC topographical profiles for each ROI, i.e., the FCs between a given ROI and all other ROIs. Then, the correlations between the FC topographical profiles of any ROI pairs were computed, which produced first-level of higher order FC networks. Through this method, researchers could generate many levels of higher-order FC networks. Previous studies showed that multi-level, high-order FC network representation could nicely capture complex interactions among brain regions. Moreover, features derived from higher-order FC networks could be used in ASD diagnosis with high accuracy (Zhao et al. 2018, 2020). In the future studies, we could generate higher-order FC networks using the DCC technique, which has higher test–retest reliability compared to the traditional Pearson's correlation approach.

On the other hand, it should be noted that the dynamic FCs between cortical ROIs not only could provide metrics that quantifying the temporal variability of FC, but also could be used to derive the temporal metrics (e.g., mean duration, time coverage, occurrence frequency and transition probability) of certain brain states through clustering analysis (Li et al. 2020). In the future studies, the DCC techniques could be used to derive such large-scale brain states, which should provide some results with higher temporal resolution and test–retest reliability.

Conclusion

In the current study, using the DCC technique and the resting-state fMRI datasets of ABIDE, the temporal dynamic features (i.e., mean and variance) of DMN-FC of ASD group and TD group were investigated. The results indicated that compared to TD participants, the mean dFC value of certain connections were significantly lower in patients with ASD, and the variance of dFC of certain connections were significantly higher in these patients. Further analysis showed that these alterations were significantly associated with symptom severity, especially the level of impaired communication skills and repetitive behaviors. These results proved and further developed the theory that aberrant temporal dynamic of FC pattern within DMN is inherent in autistic brain.

Author's contribution HJ: conceptualization, methodology, formal analysis, writing—original draft. XW: formal analysis, writing—original draft. EW: supervision, funding acquisition, writing—review and editing.

Funding The work was supported by the Philosophy and Social Sciences Planning Project of Henan Province under Grant 2020BJY010 and Henan University Philosophy and Social Science Innovation Team under Grant 2019CXTD009.

Availability of data and materials The datasets of the current study are available at https://fcon_1000.projects.nitrc.org/indi/abide/abide_I.html.

Code availability The MATLAB code here is available from the corresponding author, Dr. Huibin Jia, upon reasonable request.

Declarations

Conflict of interest The authors have no relevant financial or non-financial interests to disclose.

Ethical approval The experimental procedures were carried out in accordance with the basic principles of the Helsinki declaration and approved by the local research ethics committees.

Consent to participate All participants gave their written informed consent.

Consent for publication Written informed consent for publication was obtained from all participants.

References

Amaral DG, Schumann CM, Nordahl CW (2008) Neuroanatomy of autism. Trends Neurosci 31:137–145

Anagnostou E, Taylor MJ (2011) Review of neuroimaging in autism spectrum disorders: what have we learned and where we go from here. Mol Autism 2:4

Andrews-Hanna JR, Reidler JR, Sepulcre J, Poulin R, Buckner RL (2010) Functional-anatomic fractionation of the brain's default network. Neuron 65:550–562

Ashburner J (2007) A fast diffeomorphic image registration algorithm. NeuroImage 38:95–113

Ashburner J, Friston KJ (2005) Unified segmentation. NeuroImage 26:839–851

Auger SD, Maguire EA (2013) Assessing the mechanism of response in the retrosplenial cortex of good and poor navigators. Cortex 49:2904–2913

Baio J et al (2018) Prevalence of autism spectrum disorder among children aged 8 years—autism and developmental disabilities monitoring network, 11 sites, United States, 2014. MMWR Surveill Summ 67:1–23

Choe AS et al (2017) Comparing test-retest reliability of dynamic functional connectivity methods. NeuroImage 158:155–175

Di Martino A, Yan CG, Denio E, Castellanos FX, Alaerts K, Anderson JS (2014) The autism brain imaging data exchange: towards a large-scale evaluation of the intrinsic brain architecture in autism. Mol Psychiatry 19:659–667

Falahpour M et al (2016) Underconnected, but not broken? Dynamic functional connectivity MRI shows underconnectivity in autism is linked to increased intra-individual variability across time. Brain Connect 6:403–414

Friston KJ, Holmes AP, Worsley KJ, Poline JP, Frith CD, Frackowiak RSJ (1995) Statistical parametric maps in functional imaging: a general linear approach. Hum Brain Mapp 2:189–210

Friston KJ, Williams S, Howard R, Frackowiak RSJ, Turner R (2008) Movement-related effects in fMRI time-series. Magn Reson Med 35:346–355

Goelman G, Dan R, Stobel G, Tost H, Meyer-Lindenberg A, Bilek E (2019) Bidirectional signal exchanges and their mechanisms during joint attention interaction—a hyperscanning fMRI study. NeuroImage 198:242–254

Jung M et al (2014) Default mode network in young male adults with autism spectrum disorder: relationship with autism spectrum traits. Mol Autism 5:35

Kana RK et al (2015) Aberrant functioning of the theory-of-mind network in children and adolescents with autism Mol. Autism 6:59

Keehn B, Shih P, Brenner LA, Townsend J, Müller RA (2013) Functional connectivity for an "Island of sparing" in autism spectrum disorder: an fMRI study of visual search. Hum Brain Mapp 34:2524–2537

Lawrence KE, Hernandez LM, Bookheimer SY, Dapretto M (2019) Atypical longitudinal development of functional connectivity in adolescents with autism spectrum disorder. Autism Res 12:53–65

Lee SL, Lew D, Wickenheisser V, Markus EJ (2019) Interdependence between dorsal and ventral hippocampus during spatial navigation. Brain Behav 9:e01410

Leech R, Smallwood J (2019) Chapter 5—The posterior cingulate cortex: insights from structure and function. In: Duyckaerts C, Litvan I (eds) Handbook of clinical neurology, vol 166. Elsevier, Amsterdam, pp 73–85

Leigh JP, Du J (2015) Brief report: forecasting the economic burden of autism in 2015 and 2025 in the United States. J Autism Dev Disord 45:4135–4139

Li Y, Zhu Y, Nguchu BA, Wang Y, Wang H, Qiu B, Wang X (2020) Dynamic functional connectivity reveals abnormal variability and hyper-connected pattern in autism spectrum disorder. Autism Res 13:230–243

Murphy K, Birn RM, Handwerker DA, Jones TB, Bandettini PA (2009) The impact of global signal regression on resting state correlations: are anti-correlated networks introduced? NeuroImage 44:893–905

Padmanabhan A, Lynch CJ, Schaer M, Menon V (2017) The default mode network in autism. Biol Psychiatry Cogn Neurosci Neuroimaging 2:476–486

Sabariego M, Tabrizi NS, Marshall GJ, Mclagan AN, Jawad S, Hales JB (2020) In the temporal organization of episodic memory, the hippocampus supports the experience of elapsed time. Hippocampus 31:46–55

Shalom DB (2009) The medial prefrontal cortex and integration in autism. Neuroscientist 15:589–598

Song XW et al (2011) REST: a toolkit for resting-state functional magnetic resonance imaging data processing. PLoS ONE 6:e25031

Sun JW, Fan R, Wang Q, Wang QQ, Jia XZ, Ma HB (2021) Identify abnormal functional connectivity of resting state networks in Autism spectrum disorder and apply to machine learning-based classification. Brain Res 1757:147299

Vann SD, Aggleton JP, Maguire EA (2009) What does the retrosplenial cortex do? Nat Rev Neurosci 10:792–802

Vargas T, Damme KSF, Hooker CI, Gupta T, Cowan HR, Mittal VA (2019) Differentiating implicit and explicit theory of mind and associated neural networks in youth at clinical high risk (CHR) for psychosis. Schizophr Res 208:173–181

Walsh M, Wallace G, Gallegos S, Braden B (2021) Brain-based sex differences in autism spectrum disorder across the lifespan: a systematic review of structural MRI, fMRI, and DTI findings. NeuroImage Clin 31:102719

Yan CG, Zang YF (2010) DPARSF: a MATLAB toolbox for "pipeline" data analysis of resting-state fMRI. Front Syst Neurosci 4:13

Zalesky A, Fornito A, Bullmore ET (2010) Network-based statistic: identifying differences in brain networks. NeuroImage 53:1197–1207

Zhang H et al (2016) Topographical information-based high-order functional connectivity and its application in abnormality detection for mild cognitive impairment. J Alzheimers Dis 54:1095–1112

Zhang H, Chen X, Zhang Y, Shen D (2017) Test–retest reliability of "high-order" functional connectivity in young healthy adults. Front Neurosci 11:439

Zhao F, Zhang H, Rekik I, An Z, Shen D (2018) Diagnosis of autism spectrum disorders using multi-level high-order functional networks derived from resting-state functional MRI. Front Hum Neurosci 12:184

Zhao F, Chen Z, Rekik I, Lee SW, Shen D (2020) Diagnosis of autism spectrum disorder using central-moment features from low- and high-order dynamic resting-state functional connectivity networks. Front Neurosci 14:258